Research Square

Preprints are preliminary reports that have not undergone peer review.
They should not be considered conclusive, used to inform clinical practice,
or referenced by the media as validated information.

PINK1-dependent Mitophagy Mediates CD8+ T Cell Residency and Drives Psoriatic Relapse via CCR4-CCL17/22 Recruitment

Juan Du

dujuan@huashan.org.cn

Huashan Hospital Affiliated with Fudan University https://orcid.org/0000-0002-1327-820X

Lanmei Lin

Huashan Hospital Affiliated with Fudan University

Canbin Dong

Huashan Hospital Affiliated with Fudan University

Xinyi Zhu

Huashan Hospital Affiliated with Fudan University

Chenghui Zheng

Fudan University

Jui-Ming Lin

Huashan Hospital Affiliated with Fudan University

Huiyu Huang

Huashan Hospital Affiliated with Fudan University

Junhao Zhu

Huashan Hospital Affiliated with Fudan University

Jiazheng Sun

Huashan Hospital Affiliated with Fudan University

Xiaonian Lu

Huashan Hospital Affiliated with Fudan University

Yilun Wang

Fudan University

Huijie Zheng

Huashan Hospital Affiliated with Fudan University

Jinhua Xu

Huashan Hospital Fudan University https://orcid.org/0000-0002-2725-4903

Article

Keywords: Psoriasis, Mitophagy, Recurrence, Tissue-resident memory T cells (TRM), CCR4

Posted Date: September 17th, 2026

DOI: https://doi.org/10.21203/rs.3.rs-10912733/v1

License: This work is licensed under a Creative Commons Attribution 4.0 International License.
Read Full License

Additional Declarations: (Not answered)

Abstract

Psoriasis is a chronic inflammatory skin disease characterized by the tendency to relapse in situ. While $CD8^+$ tissue-resident memory T cells are key mediators of recurrence, the mechanisms sustaining their persistence remain unclear. This study investigates whether PINK1-mediated mitophagy, orchestrated by the CCR4–CCL17/22 signaling axis, promotes $CD8^+$ T cell residency. Utilizing single-cell and spatial transcriptomics, multiplex immunofluorescence on human lesions, and imiquimod-induced models in *Pink1*knockout mice, we found that PINK1-mediated mitophagy is significantly upregulated during occurrence and relapse phases. High mitophagy signatures in $CD8^+$ T cells correlated with increased residency. We demonstrated that epidermal Langerhans cell 2 (LC2) and $CD8^+$ T cells interact via CCR4 and its ligands CCL17/22. Functional assays confirmed this LC2-CCR4 axis sustains $CD8^+$ T-cell residency by driving PINK1-dependent mitophagy. Disruption of this pathway dismantled T cell persistence and alleviated recurrence in situ in murine models. In conclusion, PINK1-mediated mitophagy is a fundamental metabolic mechanism governing $CD8^+$ T cell residency. Elucidating the LC2-CCL17/22-CCR4 spatial and metabolic regulatory axis offers a mechanistic foundation for targeting mitophagy to break the cycle of psoriasis relapse.

Introduction

Psoriasis is a chronic, relapsing inflammatory skin disorder characterized by frequent recurrence(1). Although biologics and small-molecule targeted therapies have transformed the management of moderate-to-severe psoriasis, relapse after treatment withdrawal remains a major clinical challenge, and lesions often recur at previously affected sites(2). This in situ relapse is largely driven by local immune memory maintained by tissue-resident memory T (TRM) cells within the cutaneous microenvironment(3, 4). $CD8^+$ TRM cells, marked by residency-associated molecules such as CD69 and CD103, are considered a key memory subset involved in localized recurrence(5). Upon environmental stress or local antigen exposure, these cells can rapidly produce pro-inflammatory cytokines, including interleukin-17A (IL-17A) and interferon-γ(IFN-γ), thereby reinitiating the inflammatory cascade(6, 7). Thus, disrupting $CD8^+$ T cell residency may represent a practical strategy for preventing in situ relapse of psoriasis.

Long-term T cell residency in the metabolically demanding microenvironment of psoriatic lesions requires substantial metabolic adaptation(8). Mitochondria are central to cellular bioenergetics and signal transduction, and mitochondrial integrity is therefore critical for the survival and phenotypic stability of immune cells(9). Mitophagy, a selective autophagic process that removes damaged mitochondria and preserves metabolic homeostasis, has an important role in memory T cell survival(10). However, whether mitophagy contributes to $CD8^+$ T cell residency and subsequent psoriasis recurrence remains unclear.

In addition to intrinsic metabolic programming, the establishment and maintenance of T cell immune memory are shaped by the tissue microenvironment through spatial and chemotactic cues(11, 12). T cell infiltration and localization are tightly regulated by chemokine networks. Among these molecules, CCR4

is an important receptor associated with circulating memory T cells and their migration to the skin(5, 13). Psoriatic lesions show increased expression of CCR4 and its ligands, and the frequency of circulating $CD8^+CD103^+CCR4^+$ TRM cells has been linked to disease severity(14, 15). Our preliminary analyses further indicated that CCR4 expression is strikingly elevated in T cell subsets characterized by hyperactive mitophagy signatures.

On this basis, we hypothesized that CCR4 signaling may have functions beyond classical chemotactic homing after T cells enter the skin, acting as a microenvironmental signal that supports metabolic adaptation. In this study, we tested whether CCR4 activation promotes PINK1-mediated mitophagy, thereby sustaining $CD8^+$ T cell residency and contributing to in situ relapse of psoriasis. By defining this chemokine-mitophagy link, we aimed to identify a targetable mechanism underlying localized immune memory and psoriatic recurrence.

Results

1. PINK1-Dependent Mitophagy Promotes $CD8^+$ T Cell Residency and Exacerbates Psoriasis Recurrence *In Situ*.

To investigate the cellular landscape and metabolic state of the psoriatic microenvironment, we first performed a comprehensive single-cell transcriptomic analysis on human skin tissues. Unsupervised clustering and Uniform Manifold Approximation and Projection (UMAP) identified distinct major cell lineages, including Keratinocytes, Fibroblasts, T cells, Endothelial cells, Macrophages, and Dendritic cells (Figure 1A, Fig. S1A-C). The identity of these cell populations was confirmed by the robust expression of canonical marker genes (Figure 1B). UMAP projection split by sample origin highlighted the distinct cellular distributions between psoriatic lesions and non-lesional skin (Fig. S1D).

Calculating mitophagy-related gene (see Appendix S1) module scores across the single-cell landscape revealed that mitophagy signatures were prominently enriched in the lesional samples (Fig. S1E). Stratification of T cells based on their mitophagy-related gene expression demonstrated that T cells with high mitophagy signatures (mitophagy-high) expressed markedly increased levels of the residency markers *CD69* and *ITGAE* (*CD103*) compared to mitophagy-low T cells (Figure 1C).

Consistent with these transcriptomic findings, immunofluorescence confirmed elevated PINK1 expression in psoriatic lesions, with residual expression in the non-lesional skin compared with controls (Figure 1D-E). However, BNIP3 showed no obvious residual expression after disease resolution (Figure S1F-G), suggesting that PINK1-mediated mitophagy is key to the *in situ* recurrence of psoriatic lesions. To delve deeper into the microenvironment, we further extracted specific cellular subsets from psoriatic lesions and non-lesional skin for high-resolution re-clustering (Figure 1F). Within the refined TRM populations, we similarly observed sustained high *PINK1* expression (Figure 1G-H). Spatial transcriptomic analysis of psoriatic lesions revealed that the expression regions of *PINK1* highly overlapped with those of *CD69* and *ITGAE*, which are highly expressed on tissue-resident T cells (Figure

1I). Multiplex immunofluorescence of psoriatic lesions from patients also demonstrated the *in situ* co-localization of PINK1 with CD69 and CD103 (Figure 1J).

We used T0467 and ABT737 to activate the PINK1-Parkin pathway, as both compounds are validated activators of mitophagy via this route(16, 17). We isolated $CD8^+$ T cells from the peripheral blood of psoriasis patients for the experiments (Figure 2A). Pharmacological activation of the PINK1-Dependent pathway in patient-derived $CD8^+$ T cells induced intracellular mitophagosome formation (Figure S1H), upregulated *CD69* and *CD103* mRNA (Figure 2B-E), and increased the frequency of $CD8^+$, $CD69^+$ and $CD103^+$ T cells (Figure 2F-I). Notably, in the high-dose ABT737 group, the proportion of $CD8^+CD103^+$ T cells increased from approximately 8.32% in the control group to 15.56%.

In vivo, this study utilized wild-type C57BL/6 mice and *Pink1* heterozygous knockout ($Pink1^{+/-}$) mice to establish a mouse model of psoriasis recurrence (Figure 3A). The verification of the $Pink1^{+/-}$ heterozygous knockout is shown in Figure S2. $Pink1^{+/-}$mice exhibited reduced severity of psoriatic lesion, with lower erythema, scaling, and infiltration scores (Figure 3B, S3), and decreased PASI and skin thickness (Figure 3C-D) during both the onset and recurrence phases. H&E staining results showed that during the recurrence phase, the ear skin of wild-type mice exhibited typical psoriasis-like pathological changes: acanthosis, hyperkeratosis, and massive inflammatory cell infiltration in the dermis. In contrast, the pathological changes in the lesional tissue of $Pink1^{+/-}$ mice were milder (Figure 3E). Transmission electron microscopy was used to observe the ultrastructure of mitochondria in the recurrent lesions of the mice. It was found that mitochondria in the recurrent lesions of wild-type mice exhibited the irregular morphology and swelling common under inflammatory conditions, but the structures remained relatively dense. In *Pink1* knockout mice, typical mitochondrial damage phenotypes were observed, including mitochondrial swelling, disorganized cristae arrangement, and matrix vacuolization (Figure 3F), which may be related to the partial inhibition of the damaged mitophagy pathway caused by the *Pink1* heterozygous knockout. To investigate the effect of *Pink1* heterozygous knockout on $CD69^+$ and $CD103^+$ T cells in the tissue, we analyzed the psoriasis-like lesions of mice in different groups during the recurrence phase using RT-qPCR and immunofluorescence staining. The knockout of *Pink1* similarly reduced CD69 and CD103 expression in the psoriasis-like lesions during both the onset and recurrence phases (Figure 3 G-K).

Furthermore, activation of the PINK1-dependent mitophagy with ABT737 aggravated lesion in mice during both onset and relapse (Figure 4A-D, S4), with consistent histological changes (Figure 4E). Transmission electron microscopy results confirmed that ABT737 pharmacologically activated mitophagy(Figure 4F): in the ABT737 intervention group, clustered mitophagosomes were observed in psoriasis-like lesions. Meanwhile, RT-qPCR and immunofluorescence confirmed a significant increase in the expression of CD69 and CD103 in lesional skin (Figure 4G-K). Taken together, these findings suggest that PINK1-dependent mitophagy promotes $CD8^+$ T-cell residency and is associated with exacerbation of psoriatic recurrence in experimental models.

2. CCR4 Identifies a Pathogenic T-Cell Subtype Characterized by Hyperactive Mitophagy.

Based on the mitophagy-related gene set scores, T cells within the psoriatic lesions were divided into a high mitophagy group and a low mitophagy group (Supporting information_genesets). Within the single-cell dataset, *CCR4* expression was upregulated in T cells with high mitophagy signatures (Figure 5A), suggesting that CCR4 might be a key receptor for maintaining the high mitophagy state of T cells. To confirm the association between CCR4 and mitophagy, we further stratified the T cells into two functional subpopulations based on *CCR4* expression levels: a high *CCR4* expression (*CCR4*^{hi}) subtype and a low *CCR4* expression (*CCR4*^{lo}) subtype (Figures 5B-C).

Stratification of lesional T cells into *CCR4*^{hi} *and CCR4*^{lo} *subsets, followed by differential expression analysis, reveal*ed enrichment of genes involved in mitophagy, memory T-cell differentiation, Th17 cell differentiation, IL-17 signaling, and intercellular adhesion (Figures 5D-E). Scoring of mitophagy-related activity further demonstrated significantly higher mitophagy in *CCR4*^{hi} compared with *CCR4*^{lo} T cells (Figure 5G). To investigate the function of CCR4^{+} T cells in psoriasis recurrence, single-cell transcriptomic analysis of psoriatic lesions and non-lesional skin revealed increased *CCR4* expression in psoriatic lesions compared with non-lesional and healthy skin (Figure 5F). Immunofluorescence of patients' biopsies confirmed elevated CCR4 in lesional skin (Figure 5H).

In psoriatic lesional tissues, the high transcription regions of the *CCR4* and *CD8* genes exhibited spatial correlation with the residency marker *CD69*. More crucially, the expression distribution of *PINK1*, a key molecule in mitophagy, also partially overlapped with the *CCR4*-positive regions (Figure 5I). Given that PINK1 was demonstrated to co-localize with CD69 and CD103 in the immunofluorescence staining results from the first part of this study, we further performed multiplex immunofluorescence analysis of CCR4, CD8, and PINK1 in psoriatic lesional tissues. The results showed that CD8+ T cells exhibited partial co-localization with CCR4 and PINK1 (Figure 5J).

3. CCR4 Blockade Attenuates PINK1-Dependent Mitophagy and Disrupts Mitochondrial Homeostasis.

To investigate whether CCR4 influences mitophagy, CD8^{+} T cells from the peripheral blood of psoriasis patients were treated with the CCR4 inhibitor AZD2098 (Figure 6A). Typical mitochondrial damage could be observed in the cells of the AZD2098 group (high-concentration group), including mitochondrial swelling, matrix vacuolization, and loss of cristae (Figure 6B), which is considered to be associated with the accumulation of damaged mitochondria caused by the blocked mitophagy process. The mitochondrial membrane potential (ΔΨm), measured by JC-1 staining, was decreased in the high-dose AZD2098 treatment group compared to the control group (JC-1: 6.90 vs 3.00), indicating a loss of mitochondrial membrane potential (Figure 6C), which is consistent with the accumulation of damaged mitochondria in the AZD2098 group observed in the previous electron microscopy results. Meanwhile, compared with the untreated control group, intracellular ATP levels were decreased after AZD2098 treatment (Figure 6D). The above morphological and functional data collectively suggest that the loss of CCR4 signaling results in the inability to clear damaged mitochondria in CD8^{+} T cells in a timely manner,

leading to their accumulation. To further investigate the mitophagy levels of $CD8^+$ T cells before and after AZD2098 inhibitor intervention, we used immunofluorescence staining to detect the co-localization of TOMM20 (a mitochondrial marker) and LC3 (an autophagy motif marker). As shown in Figure 6E, after AZD2098 treatment, the co-localization of TOMM20 and LC3 in $CD8^+$ T cells was reduced, confirming that mitophagy was inhibited.

We further examined the classical PINK1/Parkin mitophagy axis. Normally, mitochondrial depolarization induces the rapid accumulation of PINK1 protein on the outer membrane, which subsequently recruits and phosphorylates cytosolic Parkin protein to initiate mitophagy(18). Following AZD2098 intervention, the expression levels of *PINK1* mRNA and PINK1 protein were downregulated; meanwhile, changes in the mRNA and protein expression levels of the downstream effector molecule Parkin showed no statistical significance (Figures 6F-H, S5A-B). These *in vitro* data collectively suggest that blocking CCR4 inhibits the expression of PINK1, rather than uniformly downregulating both PINK1 and Parkin molecules. The stagnation of the mitophagy process ultimately triggers the intracellular accumulation of damaged mitochondria and metabolic dysfunction. Furthermore, RT-qPCR results showed that after AZD2098 intervention, there was no statistical difference in the mRNA expression of classical genes of the receptor-mediated mitophagy pathway (*BNIP3* and *BNIP3L*) in $CD8^+$ T cells (Figures S5 C-D).

4. CCR4 Blockade Alleviates Psoriasis Relapse by inhibitingMitophagy-Dependent T-Cell Residency.

In vitro, $CD8^+$ T cells isolated from the peripheral blood of psoriasis patients and treated with AZD2098 showed reduced CD69 and CD103 expression (Figure 6 I-J□7A-D). This was accompanied by markedly reduced production of IL-17 and IFN-γ in $CD8^+CD69^+$ and $CD8^+CD103^+$ TRM subsets (Figure 7E-J). To determine whether CCR4-dependent residency required mitophagy, CCR4 inhibition was combined with activation of PINK1/Parkin using T0467 or ABT737. Mitophagy activation restored CD69 and CD103 expression in $CD8^+$ T cells despite CCR4 blockade (Figure 7K-P).

In a murine model of psoriasis relapse, treatment with the CCR4 inhibitor AZD2098 significantly alleviated the severity of skin lesions during both the initial onset and recurrence (Figure 8A-B, S6). CCR4 expression persisted in skin tissue after lesion regression and further increased during recurrence (Figure 8C). In addition to ameliorating the clinical features of IMQ-induced psoriasis-like lesions—including erythema, scaling, infiltration, PASI scores, and skin thickness (Figures S5E-F)—the time-score curve showed that AZD2098 administration maintained a lower disease activity throughout the entire disease cycle (Figure 8D). Histological analysis confirmed attenuated epidermal thickening and inflammatory infiltration (Figure 8F). Consistent with these findings, the lesional expression of the T cell's resident markers CD69 and CD103 was significantly downregulated (Figures 8G-H).

We further utilized transmission electron microscopy and immunofluorescence staining to confirm the blockade effect of CCR4 inhibition on the mitophagy pathway *in vivo*. Transmission electron microscopy observation showed that in the lesional skin of the psoriasis control group mice, the electron density of the mitochondrial matrix was relatively uniform, and typical double-membrane mitophagosome

structures were visible in the cytoplasm. Conversely, pathological changes in mitochondria were observed in the AZD2098 group: mitochondria were generally swollen, the electron density of the matrix was low, and the mitochondrial cristae structures were blurred or fractured (Figure 8E). This pathological morphology is consistent with the *in vitro* experiments, suggesting that CCR4 inhibition also blocks the normal clearance pathway of damaged mitochondria *in vivo*. To further confirm the specific pathway through which CCR4 regulates mitophagy, we examined the expression changes of key molecules from different mitophagy pathways in the psoriasis-like recurrent lesions. Immunofluorescence staining confirmed decreased PINK1, but not BNIP3, following CCR4 inhibition (Figures 8I-J, S5G). These results suggest that CCR4 inhibition attenuates PINK1-dependent mitophagy in $CD8^+$ T cells and ameliorates psoriasiform inflammation *in vivo*. These results indicate that CCR4 inhibition limits $CD8^+$ T cell residency and reduces psoriasiform relapse, and that this effect can be conteracted by mitophagy activation.

5. Interaction Between LC2 and $CCR4^+$ T Cells Supports Residency Accumulation *In Situ*.

Interestingly, analysis of peripheral blood from psoriasis patients and healthy controls revealed that the frequency of circulating $CCR4^+$ T cells was significantly lower in patients (Figures 9A-B). Furthermore, this frequency negatively correlated with disease severity (Figure 9C), suggesting that the reduction of circulating $CCR4^+$ T cells suggests their recruitment into the lesional skin. Additionally, bioinformatic analysis of single-cell and public transcriptomic datasets (GSE248121 and GSE151177), combined with immunofluorescence validation, confirmed elevated levels of the CCR4 ligands CCL17 and CCL22 in psoriatic lesions. This aligns with the previously observed upregulation of CCR4 in these localized areas (Figures 9E, S7A, C-D, S8-9). Notably, these ligands were found to be primarily derived from LC2 (Langerhans cell 2) populations (Figures 9F-G, S7B). Consistently, immunofluorescence staining also demonstrated an upregulated expression of the LC2 marker CD63 in the skin of patients (Figures 9H-I). To further elucidate the *in situ* interaction between LC2 and the recruited T cells, we performed spatial transcriptomics analysis on psoriatic lesions. Spatial mapping revealed that LC2 ($CD63^+CLEC10A^+$) and $CCR4^+$ T cells were not randomly dispersed but formed dense, highly selective spatial clusters within the lesional architecture(Figure 9J). Quantitative neighborhood analysis demonstrated that individual LC2 spots were robustly surrounded by a high density of $CCR4^+$ T cells, establishing a highly structured chemotactic niche(Figure 9J). Crucially, these LC2-$CCR4^+$ T cell spatial clusters profoundly overlapped with the spatial distribution of TRM cells expressing classical residency markers ($CD3^+CD69^+ITGAE^+$) (Figure 9K,S 7E). This striking spatial co-localization strongly implies that the LC2-orchestrated localized microenvironment not only mediates the targeted recruitment of $CCR4^+$ T cells but also fundamentally supports their subsequent phenotypic transition into a permanent resident state.

Discussion

In-situ relapse remains a formidable challenge in the clinical management of psoriasis, fundamentally driven by the persistent residency of $CD8^+$ pathogenic T cells within the lesional microenvironment(3,

19). Herein, our study delineates a previously unappreciated immuno-metabolic regulatory axis—the CCR4-PINK1-mitophagy cascade—which intricately integrates localized spatial signals with cell-intrinsic metabolic reprogramming to dictate the long-term persistence of $CD8^+$ T cells in psoriatic lesions.

The main advance of this study is the functional transition of CCR4 from a canonical chemotactic receptor to an essential metabolic regulator upon entering the skin. We demonstrate that CCR4 signaling is obligate for maintaining PINK1-dependent mitophagy in $CD8^+$ T cells. Our experimental results reveal that CCR4 blockade profoundly downregulates PINK1 expression and impedes its mitochondrial accumulation, precipitating a failure to clear damaged mitochondria and inducing severe metabolic dysfunction, characterized by morphological abnormalities and ATP depletion. Crucially, we demonstrate that hyperactive mitophagy is not merely an epiphenomenon of inflammation but a pathogenic driver; heightened PINK1-mediated mitophagy directly exacerbates the severity of psoriasiform lesion relapse. By sustaining this mitophagy, $CD8^+$ T cells maintain metabolic homeostasisrequired to adapt to severe metabolic stress, enabling their long-termresidency and fueling aggressive disease recurrence even after the resolution of initial lesional inflammation.

Beyond intracellular metabolic rewiring, the consolidation of this resident phenotype is strictly governed by structured microenvironmental niches. Within the highly organized lesional architecture, spatial transcriptomic analysis confirmed a pronounced spatial proximity between the chemokine-secreting Langerhans cell 2 (LC2) and $CCR4^+$ T cells. Notably, CCL17 and CCL22—which are highly expressed by the LC2—serve as highly selective ligands for CCR4, facilitating the precise recruitment and spatial anchoring of T cells(20). Our data delineate that LC2 and $CCR4^+CD8^+$ T cells form highly selective spatial clusters, providing the molecular and structural architecture for T-cell positioning within the epidermis. Quantitative neighborhood analysis further reveals that this spatial proximity robustly overlaps with the distribution of residency markers (CD69 and CD103), demonstrating that the LC2-orchestrated chemotactic niche is indispensable for supporting the transition of T cells toward a resident phenotype.

In summary, this study provides evidence that LC2-derived chemotactic signals spatially interact with $CCR4^+CD8^+$ T cells, subsequently enforcing T-cell metabolic homeostasis through the CCR4-PINK1-mitophagy axis to promote a long-term resident phenotype. Targeting the $CCR4^+$ T cell subset or directly inhibitingits intrinsic mitophagy represents a highly promising therapeutic strategy to eradicate the localized psoriatic footprint and achieve sustained disease remission.

Materials and Methods

Human Skin Sample Collection

Skin biopsy samples were collected from patients diagnosed with chronic plaque psoriasis for immunofluorescence and single-cell transcriptome sequencing. Each participant underwent a detailed dermatological examination and was assessed by an experienced dermatologist using a severity index.

Biopsies included skin from both lesional and non-lesional areas, with samples from healthy volunteers serving as controls.

Construction of a Mouse Model of Psoriasis Recurrence and Drug Treatment

Six-week-old female BALB/c mice were purchased from Charles River Laboratories (Wilmington, MA, USA). AZD2098 and ABT737 (Selleck, Shanghai, China) were dissolved in dimethyl sulfoxide (DMSO; Sigma-Aldrich, St. Louis, Missouri, USA). The mouse model of psoriasis relapse was established as described by Shi *et al.*(21). Detailed experimental procedures and information for the Construction are provided in Appendix S1.

Flow Cytometry

For flow cytometric analysis, $3X10^5$ cells were stained with specific antibodies in PBS supplemented with 5% fetal bovine serum and 0.1% NaN3, and incubated on ice for 30 minutes. Antibodies used included CD8 (BD Pharmingen, 560662) CCR4 (Biolegend, 359433), CD69 (BD Horizon, 562884), CD103 (eBioscience, 2691691), IFN-γ (Biolegend, 502508), and IL-17 (Biolegend, 512319). After washing, cells were fixed in 2% paraformaldehyde in PBS and analyzed on a BD FACS Calibur. Data analysis was performed using FlowJo software version 5.7.1.

Pink1 heterozygous knockout mice

The schematic diagram for generating *Pink*1 heterozygous knockout mice is provided in Supplementary Fig. S2A. Through bioinformatic analysis, sgRNA sequences specifically targeting the *Pink1* gene were screened. Distinct sgRNA sequences were selected to ensure efficient targeting of critical regions within the *Pink1* gene and achieve heterozygous knockout. DNA fragments containing the *Pink1* sgRNA sequences were amplified via PCR. These fragments then served as templates for synthesizing sgRNA through in vitro transcription. Similarly, Cas9 mRNA was synthesized by in vitro transcription. A mixture of the synthesized *Pink1* sgRNAs (four sgRNAs, each at 30 ng/μl) and Cas9 mRNA (100 ng/μl) was prepared for cytoplasmic microinjection into zygotes. Healthy mouse embryos were selected, and the mixture was precisely injected into the cytoplasm using microinjection techniques. Following injection, the embryos were transplanted into surrogate mothers. After birth, genotyping was performed using tail DNA to verify the knockout efficiency (Fig. S2B-D).

Single-Cell Transcriptome Sequencing and Data Analysis

RNA was extracted from lesional and non-lesional skin samples of psoriasis patients and sequenced using 150 bp paired-end reads on a NovaSeq 6000 system (Illumina, CA, USA). Data processing was performed with Cell Ranger software (10x Genomics, CA, USA), including quality control, alignment to the hg38 reference genome, and gene quantification. The data were integrated into a combined expression

matrix using the Cell Ranger 'aggr' function. Detailed methodologies and cell annotation information are provided in Appendix S1. Transcriptome data were obtained from the GSE248121 and GSE151177; please refer to the relevant literature for specific patient information(22, 23). Spatial transcriptome sequencing data were retrieved from GSM7049132(24).

Cell Clustering and Cell Type Annotation

Cell clustering was performed using Seurat (v3.1.2), with cells displaying fewer than 500 transcripts or more than 20% mitochondrial expression, filtered out as low quality. Normalization, variable gene selection, sample integration, and scaling were conducted using default parameters of the respective functions in Seurat. Principal Component Analysis (PCA) on variable genes was followed by cell clustering and UMAP dimensionality reduction, utilizing the top 50 PCs. Clusters were delineated using FindNeighbors and FindClusters functions with cluster marker genes identified using the FindAllMarkers function. Cell types were annotated by matching cluster markers with genes typical of known cell types.

Enrichment Analysis and Cellular Interactions

Gene Ontology (GO) and Kyoto Encyclopedia of Genes and Genomes (KEGG) enrichment analyses were conducted using the R packages “enrichGO” and “enrichKEGG,” respectively. Cell-cell interaction analysis was performed with the “CellChat” package.

Mitophagy Score

3 mitochondrial autophagy gene sets were obtained for mitochondrial autophagy scoring using the “AUCell” R package(25, 26). These 3 mitochondrial autophagy sets were set as input data for area under the curve (AUC) value calculation. According to the AUC value, gene-expression rankings were built for each cell. The AUC estimates the proportion of genes in the gene set that are highly expressed in each cell. Cells expressing many genes from the gene set will have higher AUC values than cells expressing fewer genes.

Isolation and Culture of $CD8^+$ T Cells

$CD8^+$ T cells were isolated from the peripheral blood of psoriasis patients. Peripheral blood mononuclear cells were first separated by Ficoll-Hypaque density gradient centrifugation using Human Ficoll-Paque™ Plus (Cytiva, Marlborough, MAUSA). $CD8^+$ T cells were then purified using CD8 magnetic beads (Miltenyi Biotec, Bergisch Gladbach, Germany). The isolated cells were cultured in X-Vivo15 medium supplemented with 20% fetal bovine serum (FBS; Gibco, Carlsbad, CA, USA) and treated with AZD2098 (100 nM or 150 nM), T0467(10 μM or 20 μM), or ABT737 (0.5 μM or 1 μM) for 48 h.

Reverse Transcription Quantitative PCR

After culture, cells were centrifuged, and RNA was extracted using TRIzol reagent (Sigma-Aldrich, St. Louis, MO, USA) following the manufacturer's protocol. RNA was reverse-transcribed into cDNA using the Takara Reverse Transcription Kit (Takara Bio, Beijing, China) and stored at − 20°C. Quantitative PCR was performed on a 7900HT Fast Real-Time PCR System (Thermo Fisher Scientific, Waltham, MA, USA).

Mitochondrial Membrane Potential Assay

Mitochondrial membrane potential was assessed using JC-1 dye (BD, 551302). Cells were incubated with JC-1 working solution at 37°C for 15–30 minutes. In cells with high mitochondrial membrane potential, JC-1 aggregates and exhibits red fluorescence; in cells with low membrane potential, it remains in monomeric form, exhibiting green fluorescence. After incubation, cells were rinsed with PBS, and the red-to-green fluorescence ratio was measured using a fluorescence microscope or flow cytometer. A decrease in this ratio indicates impaired mitochondrial function.

ATP production assay

The ATP content was assessed using the Enhanced ATP Assay Kit (Beyotime, China). After the indicated treatments, isolated CD8 + T cells were lysed with the ATP lysis buffer. Subsequently, the supernatant was harvested through centrifugation (12,000 × g, 5 min) and subjected to a reaction with the ATP detection working solution. The luminescence activity was detected by a microplate reader (EnSpire, United States).

Transmission Electron Microscopy

Transmission electron microscopy (TEM) was used to observe cellular ultrastructure. Tissue samples were immediately fixed in 2.5% glutaraldehyde for 2–4 hours to preserve structural integrity. Post-fixation was performed with 1% osmium tetroxide to enhance membrane contrast. Samples were dehydrated through an ethanol gradient, embedded in epoxy resin, and polymerized at 60°C until fully cured. Ultrathin sections (70–90 nm) were cut using an ultramicrotome, collected on copper grids, and stained with uranyl acetate and lead citrate. Samples were then observed under a TEM to analyze organelle ultrastructure through high-resolution imaging.

Immunofluorescence Analysis

Tissue samples were fixed in 4% paraformaldehyde and incubated with primary antibodies including rabbit anti-CD69 (Absinbio, abs136297), rabbit anti-CD103(Absinbio, abs118732), rabbit anti-PINK1(Servicebio, GB114934-100), rabbit anti-Parkin (Servicebio, GB 15596-50), rabbit anti-BNIP3 (Servicebio, GB111204), and rabbit anti-CCR4 (Bioss, bs-1168R). Following overnight incubation at 4°C, samples were stained with secondary antibodies (Alexa Fluor 555 anti-rabbit IgG and Alexa Fluor 488 anti-mouse IgG, both 1:2000, Cell Signaling Technology) at room temperature. DAPI (Dako, Glostrup, Denmark) served as a nuclear counterstain. Slides were examined using a confocal laser scanning microscope (FV-1000, Olympus, Tokyo, Japan).

Western Blotting Analysis

Psoriasis patients' $CD8^+$ T cells isolated from psoriasis patients were treated with AZD2098 or vehicle control for the indicated times. Total proteins were extracted using RIPA lysis buffer supplemented with protease and phosphatase inhibitors. Protein concentrations were determined using a BCA protein assay kit. Equal amounts of protein lysates were separated by SDS-PAGE and subsequently transferred onto PVDF membranes. After blocking with 5% non-fat milk for 1 hour at room temperature, the membranes were incubated overnight at 4°C with the following primary antibodies: rabbit anti-PINK1 polyclonal antibody (Absin, abs148857), rabbit anti-Parkin monoclonal antibody (CST, #32833T), and anti-beta-Actin antibody (CST, #4967S) as the internal loading control. Following rigorous washing with TBST, the membranes were incubated with HRP-conjugated secondary antibodies for 1 hour at room temperature. The target protein bands were visualized using an enhanced chemiluminescence (ECL) detection system and quantified via ImageJ software.

Statistical Analysis

Statistical analyses were performed using the R package "stats" (version 3.6.2) and Prism software (version 8.0; GraphPad, La Jolla, CA, USA). unpaired 2-tailed t tests for 2-group comparisons or 1-way ANOVA followed by Tukey Honestly Significant Difference test for multiple comparisons. A p-value of < 0.05 was considered statistically significant.

Abbreviations

AUCell: Area Under the Curve cell rankings

CCL17/22: Chemokine (C-C motif) ligand 17 and 22

CCR4: C-C chemokine receptor type 4

$CD8^+$ T cells: Cluster of Differentiation 8 positive T cells

cDNA: Complementary DNA

CXCR3: C-X-C chemokine receptor type 3

CXCR6: C-X-C chemokine receptor type 6

DMSO: Dimethyl sulfoxide

ELISA: Enzyme-linked immunosorbent assay

FBS: Fetal bovine serum

GO: Gene Ontology

GEO: Gene Expression Omnibus

H&E: Hematoxylin and eosin

IFN-γ: Interferon-gamma

IL-17A: Interleukin-17A

IMQ: Imiquimod

KEGG: Kyoto Encyclopedia of Genes and Genomes

LC2: Langerhans cell type 2

mRNA: Messenger RNA

PBMC: Peripheral blood mononuclear cells

PASI: Psoriasis Area and Severity Index

PBS: Phosphate-buffered saline

PCR: Polymerase chain reaction

PINK1: PTEN-induced kinase 1

RT-qPCR: Reverse transcription quantitative polymerase chain reaction

TEM: Effector memory T cells

TEM: Transmission electron microscopy

TCM: Central memory T cells

TRM: Tissue-resident memory T cells

Treg: Regulatory T cells

ΔΨm: Mitochondrial membrane potential

Declarations

Acknowledgments: The Medical Science Data Center of Fudan University supports this research.

Disclosure statement: The authors declare that they have no relevant financial or non-financial conflicts of interest to disclose in relation to the content of this manuscript.

Ethics statement: The studies involving human participants were reviewed and approved by the Institutional Review Board of Huashan Hospital, Fudan University (2024-1004), and carried out in line

with the guidelines outlined in the Declaration of Helsinki. Written informed consent was obtained from all participants prior to the commencement of the study. All animal experiments were approved by the Ethics Committee of Huashan Hospital (202501025S).

Data availability: The data are included in the article and its Supporting Information. Further inquiries may be directed to the corresponding author.

Funding: This work was supported by the National Natural Science Foundation of China (82573961, 82003382 and 81673081), the Science and Technology Commission of Shanghai Municipality (No.24ZR1407800), the National Key Research and Development Program of China (2023YFC2508103), the Clinical Research Plan of SHDC (grant numbers: SHDC2020CR6022 and SHDC22022302), the Bethune Charitable Foundation (J202301E036)

References

1. Yan BX, Chen XY, Ye LR, Chen JQ, Zheng M, Man XY. Cutaneous and Systemic Psoriasis: Classifications and Classification for the Distinction. Front Med (Lausanne). 2021;8:649408.
2. Chen L, Shen Z. Tissue-resident memory T cells and their biological characteristics in the recurrence of inflammatory skin disorders. Cell Mol Immunol. 2020;17(1):64–75.
3. Zhou X, Chen Y, Cui L, Shi Y, Guo C. Advances in the pathogenesis of psoriasis: from keratinocyte perspective. Cell Death Dis. 2022;13(1):81.
4. Chen X, Zheng Y, Man X, Li W. Tissue-resident memory T cells and their function in skin diseases. Chin Med J (Engl). 2025;138(10):1175–83.
5. Dong C, Lin L, Du J. Characteristics and sources of tissue-resident memory T cells in psoriasis relapse. Curr Res Immunol. 2023;4:100067.
6. Owczarczyk Saczonek A, Krajewska-Wlodarczyk M, Kasprowicz-Furmanczyk M, Placek W. Immunological Memory of Psoriatic Lesions. Int J Mol Sci. 2020;21(2).
7. Kasprowicz-Furmanczyk M, Czerwinska J, Placek W, Owczarczyk-Saczonek A. The Effect of the Long-Term Calcipotriol/Betamethasone Dipropionate Local Therapy on Tissue Resident Memory Cells Markers in Psoriatic Eruptions. Int J Environ Res Public Health. 2022;19(14).
8. Yenyuwadee S, Sanchez-Trincado Lopez JL, Shah R, Rosato PC, Boussiotis VA. The evolving role of tissue-resident memory T cells in infections and cancer. Sci Adv. 2022;8(33):eabo5871.
9. Luo L, Lechuga-Vieco AV, Sattentau C, Borsa M, Simon AK. Dysfunctional mitochondria in ageing T cells: a perspective on mitochondrial quality control mechanisms. EMBO Rep. 2025;26(18):4402–18.
10. Franco F, Bevilacqua A, Wu RM, Kao KC, Lin CP, Rousseau L, et al. Regulatory circuits of mitophagy restrict distinct modes of cell death during memory CD8(+) T cell formation. Sci Immunol. 2023;8(87):eadf7579.

11. Dyck L, Prendeville H, Raverdeau M, Wilk MM, Loftus RM, Douglas A, et al. Suppressive effects of the obese tumor microenvironment on CD8 T cell infiltration and effector function. J Exp Med. 2022;219(3).
12. Hamaidi I, Kim S. Sirtuins are crucial regulators of T cell metabolism and functions. Exp Mol Med. 2022;54(3):207–15.
13. Teraki Y, Picker LJ. Independent regulation of cutaneous lymphocyte-associated antigen expression and cytokine synthesis phenotype during human CD4 + memory T cell differentiation. J Immunol. 1997;159(12):6018–29.
14. den Braanker H, Razawy W, Wervers K, Mus AC, Davelaar N, Kok MR, et al. Characterizing memory T helper cells in patients with psoriasis, subclinical, or early psoriatic arthritis using a machine learning algorithm. Arthritis Res Ther. 2022;24(1):28.
15. Casciano F, Diani M, Altomare A, Granucci F, Secchiero P, Banfi G, et al. CCR4(+) Skin-Tropic Phenotype as a Feature of Central Memory CD8(+) T Cells in Healthy Subjects and Psoriasis Patients. Front Immunol. 2020;11:529.
16. Jimenez-Loygorri JI, Villarejo-Zori B, Viedma-Poyatos A, Zapata-Munoz J, Benitez-Fernandez R, Frutos-Lison MD, et al. Mitophagy curtails cytosolic mtDNA-dependent activation of cGAS/STING inflammation during aging. Nat Commun. 2024;15(1):830.
17. Shiba-Fukushima K, Inoshita T, Sano O, Iwata H, Ishikawa KI, Okano H, et al. A Cell-Based High-Throughput Screening Identified Two Compounds that Enhance PINK1-Parkin Signaling. iScience. 2020;23(5):101048.
18. Imberechts D, Kinnart I, Wauters F, Terbeek J, Manders L, Wierda K, et al. DJ-1 is an essential downstream mediator in PINK1/parkin-dependent mitophagy. Brain. 2022;145(12):4368–84.
19. Benezeder T, Wolf P. Resolution of plaque-type psoriasis: what is left behind (and reinitiates the disease). Semin Immunopathol. 2019;41(6):633–44.
20. Salanga CL, Handel TM. Chemokine oligomerization and interactions with receptors and glycosaminoglycans: the role of structural dynamics in function. Exp Cell Res. 2011;317(5):590–601.
21. Lu X, Kuai L, Huang F, Jiang J, Song J, Liu Y, et al. Single-atom catalysts-based catalytic ROS clearance for efficient psoriasis treatment and relapse prevention via restoring ESR1. Nat Commun. 2023;14(1):6767.
22. Peng L, Liu W, Cheng Y, Chen L, Shen Z. IL-17A/F double producing T cells, unstable Tregs and quiescent TRMs in clinically healed lesions are potential cellular candidates for recurrence of psoriasis. Clin Immunol. 2024;266:110328.
23. Kim J, Lee J, Kim HJ, Kameyama N, Nazarian R, Der E, et al. Single-cell transcriptomics applied to emigrating cells from psoriasis elucidate pathogenic versus regulatory immune cell subsets. J Allergy Clin Immunol. 2021;148(5):1281–92.
24. Buechler MB, Pradhan RN, Krishnamurty AT, Cox C, Calviello AK, Wang AW, et al. Cross-tissue organization of the fibroblast lineage. Nature. 2021;593(7860):575–9.

25. Onishi M, Yamano K, Sato M, Matsuda N, Okamoto K. Molecular mechanisms and physiological functions of mitophagy. EMBO J. 2021;40(3):e104705.

26. [illegible]. [illegible]. 2023;27(19):1–6,11.

Figures

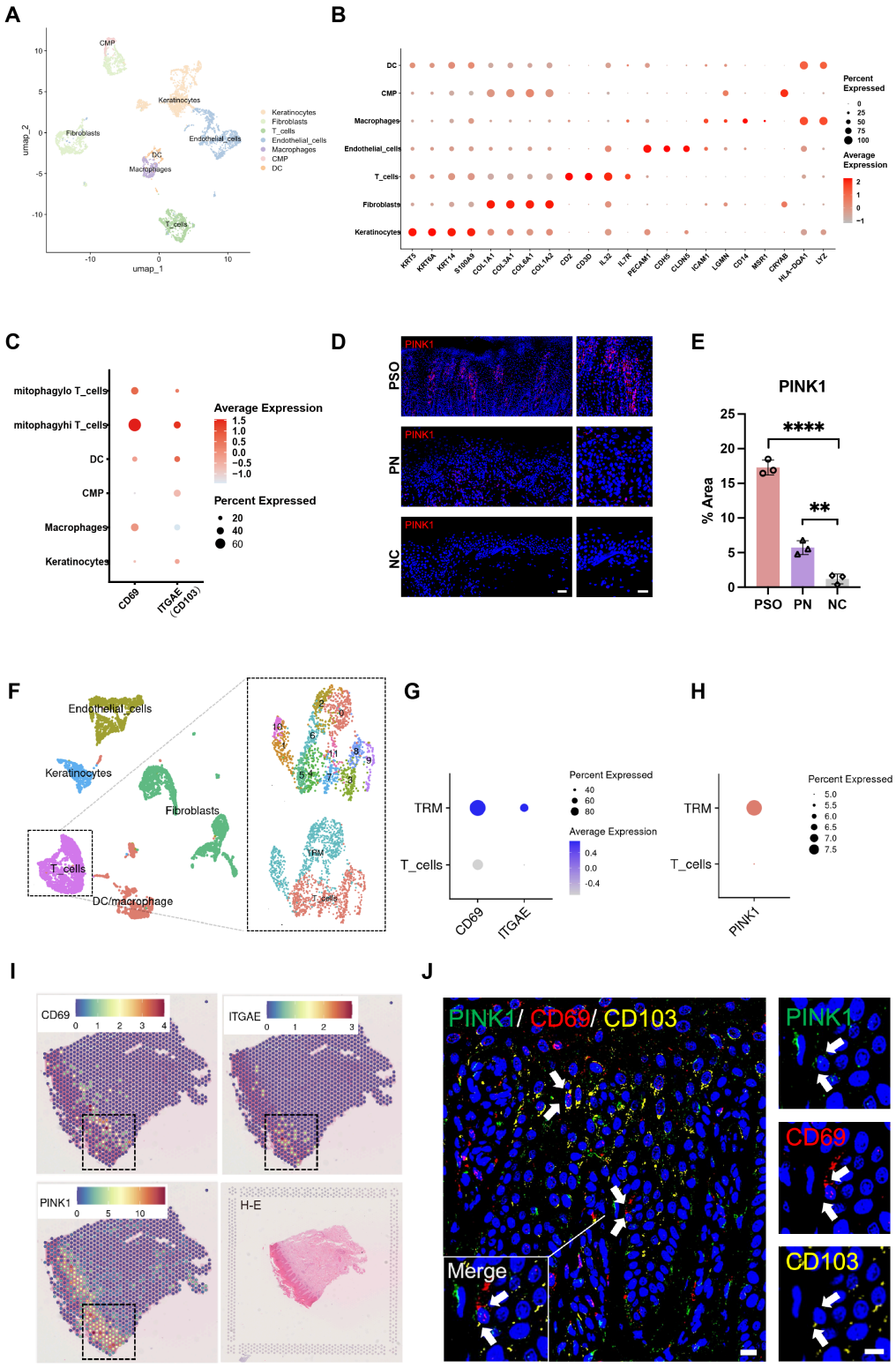

Figure 1

Single-cell and spatial transcriptomic landscapes reveal PINK1 enrichment in skin tissue-resident memory T (TRM) cells. A) UMAP embedding of single-cell RNA sequencing (scRNA-seq) data from skin tissues, identifying seven distinct major cell lineages: Keratinocytes, Fibroblasts, T cells, Endothelial cells, Macrophages, common myeloid progenitors (CMP), and dendritic cells (DC). **B)** Dot plot illustrating the average expression levels (color scale) and the percentage of expressing cells (dot size) of canonical marker genes across the identified cell clusters. **C)** Dot plot showing the expression of TRM signature genes (*CD69* and *ITGAE*) across different cell populations, highlighting their differential expression between mitophagy^{hi} and mitophagy^{lo} T cells. **D)** Representative immunofluorescence (IF) images showing PINK1 protein expression in skin lesions from psoriasis (PSO), non-lesion skin of psoriasis patients (PN), and normal control (NC) tissues. Scale bars: 50 μm, enlarged scale bar: 20 μm. **E)** Quantification of the PINK1-positive area percentage in the indicated groups from (D). Data are presented as mean ± SEM. $P < 0.01$, **** $P < 0.0001$. **F)** UMAP plot displaying the spatial distribution of major cell types (left), with a magnified view (dashed box) of the re-clustered T cell and DC/Macrophage sub-populations (right), detailing fine subsets including TRMs. **G,H)** Dot plots comparing the expression levels and expressing cell proportions of TRM markers (*CD69* and *ITGAE*) **(G)** and *PINK1* **(H)** between the TRM subset and the total T cell population. **I)** Spatial transcriptomics mapping of *CD69*, *ITGAE*, and *PINK1* transcripts in skin tissue sections. Dashed boxes indicate regions with high spatial co-localization of these target genes. **J)** Representative multiplex immunofluorescence (mIF) images evaluating the co-expression of PINK1 (green), CD69 (red), and CD103 (yellow) in skin tissue. Nuclei are stained with DAPI (blue). White arrows indicate TRM cells simultaneously expressing PINK1, CD69, and CD103. The inset (bottom left) and the isolated single-channel panels (right) provide magnified views to confirm co-localization at single-cell resolution. Scale bars: 50 μm, enlarged scale bar: 20 μm.

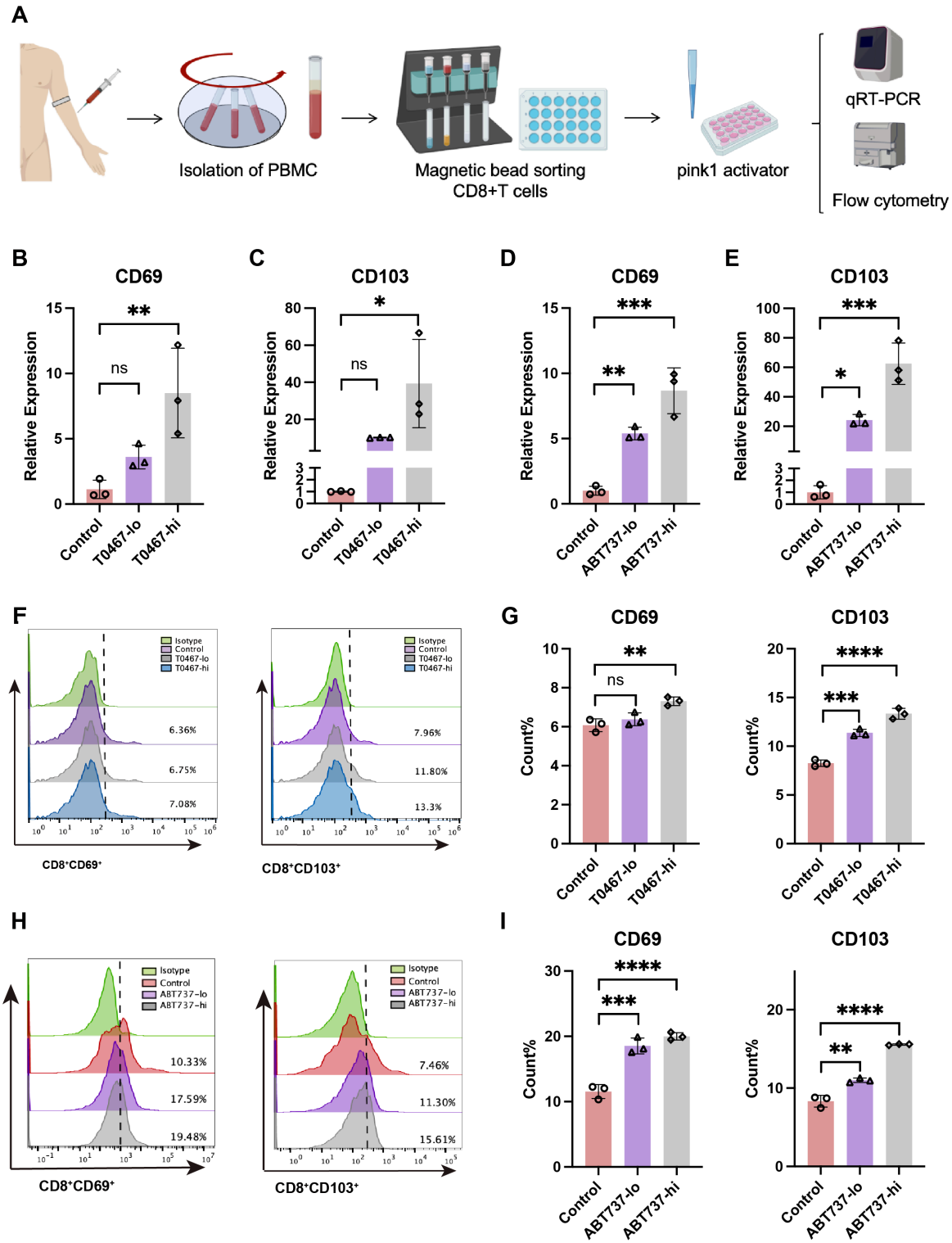

Figure 2

Pharmacological activation of PINK1 upregulates residency markers in human primary CD8$^+$ T cells. A) Schematic representation of the *in vitro* experimental workflow. Peripheral blood mononuclear cells (PBMCs) were isolated from human peripheral blood, followed by magnetic bead sorting to enrich for CD8$^+$ T cells. The purified cells were cultured and treated with PINK1 activators at varying concentrations, followed by downstream analysis using qRT-PCR and flow cytometry. **B–E)** Relative

mRNA expression levels of the T cell residency marker genes *CD69* **(B, D)** and *CD103* (also known as *ITGAE*) **(C, E)** in primary $CD8^+$ T cells treated with or without the PINK1 activator T0467 **(B, C)** or ABT737 **(D, E)** at low (-lo) and high (-hi) concentrations. Expression levels were measured by qRT-PCR and normalized to the control group. **F)** Representative flow cytometry histograms showing the surface protein expression of CD69 (left) and CD103 (right) on $CD8^+$ T cells following treatment with T0467. **G)** Statistical quantification of the percentage of $CD69^+$ and $CD103^+$ cells from panel (F). **H)** Representative flow cytometry histograms demonstrating the surface expression of CD69 (left) and CD103 (right) on $CD8^+$ T cells treated with ABT737. **I)** Statistical quantification of the percentage of $CD69^+$ and $CD103^+$ cells from panel (H). Data are presented as mean ± SEM of independent biological replicates. ns, not significant; * $P < 0.05$, ** $P < 0.01$, *** $P < 0.001$, **** $P < 0.0001$.

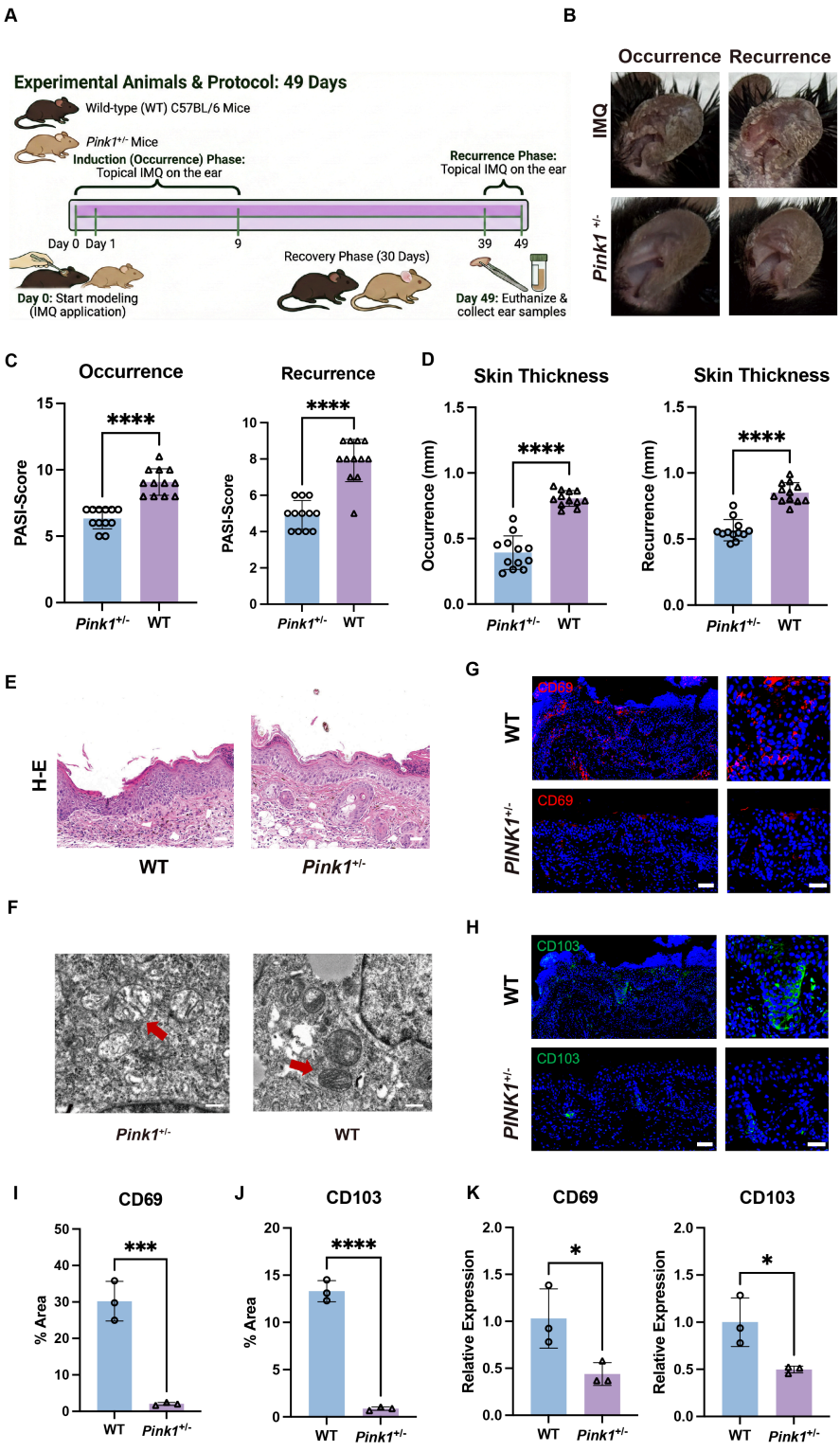

Figure 3

***Pink1* deficiency alleviates IMQ-induced psoriasis-like lesion and reduces T cell residency. A)** Schematic representation of the experimental protocol for the IMQ-induced occurrence and recurrence model. Wild-type (WT) and *Pink1* mutant mice were subjected to a 49-day timeline that included an initial IMQ topical application (occurrence phase), a 30-day recovery period, and a secondary IMQ challenge (recurrence phase). **B)** Representative macroscopic phenotypic images of the ear skin from WT and

Pink1 mutant mice during the occurrence and recurrence phases. **C,D)** Clinical evaluation of lesion severity. PASI scores **(C)** and ear skin thickness **(D)** were recorded and compared between WT and *Pink1*$^{+/-}$ mice during both the occurrence and recurrence phases. **E)** Representative H&E staining of ear skin sections from WT and *Pink1*$^{+/-}$ mice, demonstrating histological changes such as epidermal hyperplasia and inflammatory cell infiltration. **F)** Representative TEM images revealing the ultrastructural features in the skin tissues of WT and *Pink1* mutant mice. **G,H)** Representative immunofluorescence images showing the *in situ* expression of CD69 (**G**) and CD103 (**H**) in the ear skin tissues of WT and *Pink1*$^{+/-}$ mice. Scale bars: 50 μm, enlarged scale bar: 20 μm. **I,J)** Quantitative analysis of the fluorescence-positive area percentages for CD69 **(I)** and CD103 **(J)** from the respective IF images. **K)** Relative mRNA expression levels of the TRM signature genes *CD69* and *CD103* in the ear tissues of WT and *Pink1*$^{+/-}$ mice, measured via qRT-PCR and normalized to the WT group. Data are presented as mean ± SEM. * $P < 0.05$, *** $P < 0.001$, **** $P < 0.0001$.

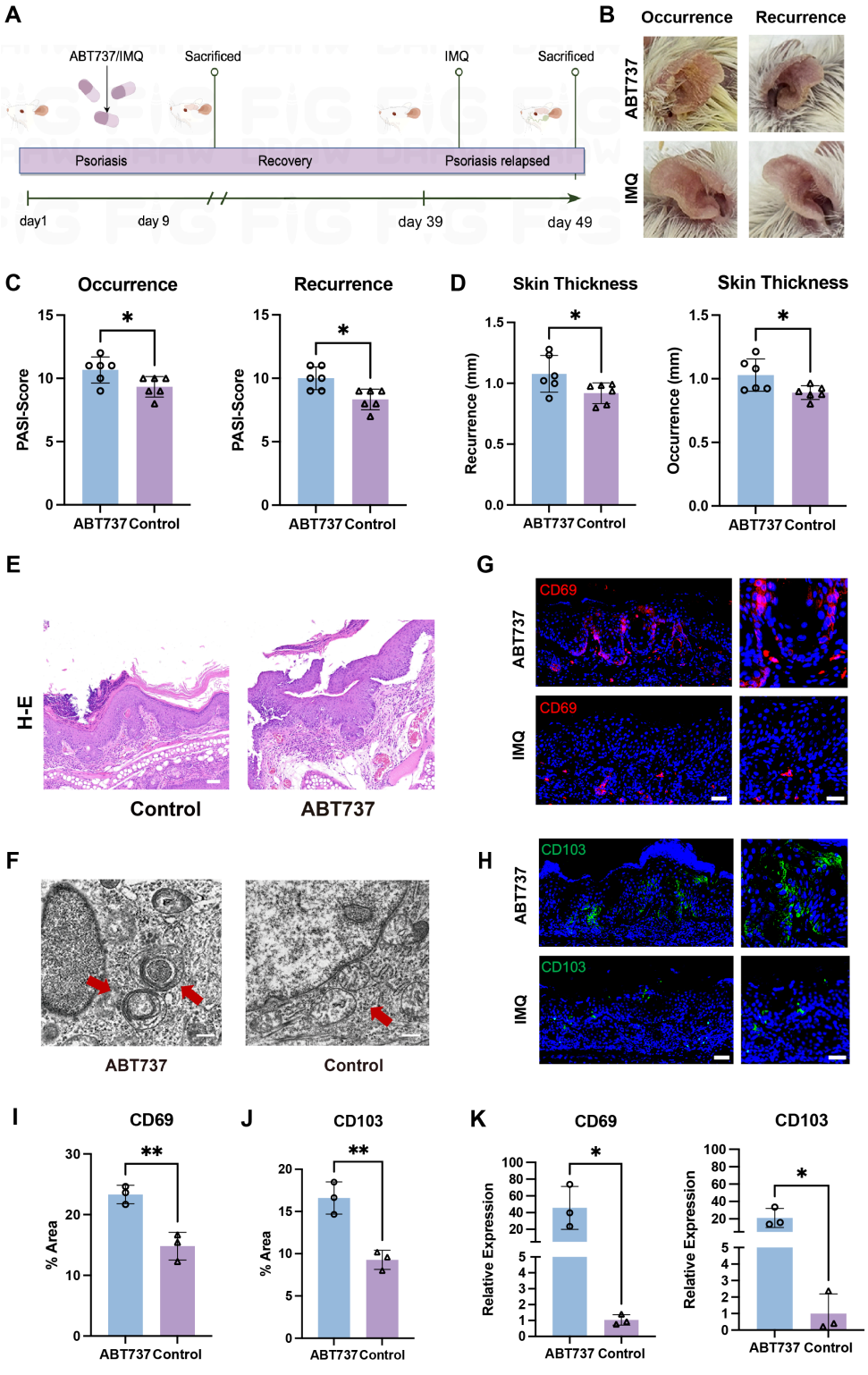

Figure 4

Pharmacological activation of PINK1 exacerbates IMQ-induced psoriasis-like lesion and promotes T cell residency *in vivo*. A) Schematic representation of the *in vivo*experimental timeline. Mice were subjected to topical IMQ application with or without the PINK1 activator ABT737 during the initial psoriasis induction (occurrence phase), followed by a recovery period and a subsequent IMQ challenge (recurrence phase). **B)** Representative macroscopic phenotypic images of the ear skin from mice treated

with ABT737 (+ IMQ) or IMQ alone during the occurrence and recurrence phases. **C, D)** Clinical evaluation of lesion severity. PASI scores **(C)** and ear skin thickness **(D)**were measured and compared between the ABT737-treated group and the Control (IMQ-only) group during both the occurrence and recurrence phases. **E)**Representative H&E staining of ear skin sections from Control and ABT737-treated mice, showing histological changes. **F)** Representative TEM images revealing ultrastructural features in the skin tissues of ABT737-treated and Control mice. **G, H)** Representative immunofluorescence images showing the *in situ* expression of CD69 (**G**) and CD103 (**H**) in the ear skin tissues. Scale bars: 50 μm, enlarged scale bar: 20 μm. **I, J)** Quantitative analysis of the fluorescence-positive area percentages for CD69 **(I)** and CD103 **(J)**from the IF images. **K)** Relative mRNA expression levels of genes *Cd69*and *Cd103* in the ear tissues of Control and ABT737-treated mice, measured via qRT-PCR and normalized to the Control group. Data are presented as mean ± SEM. * $P < 0.05$, ** $P < 0.01$.

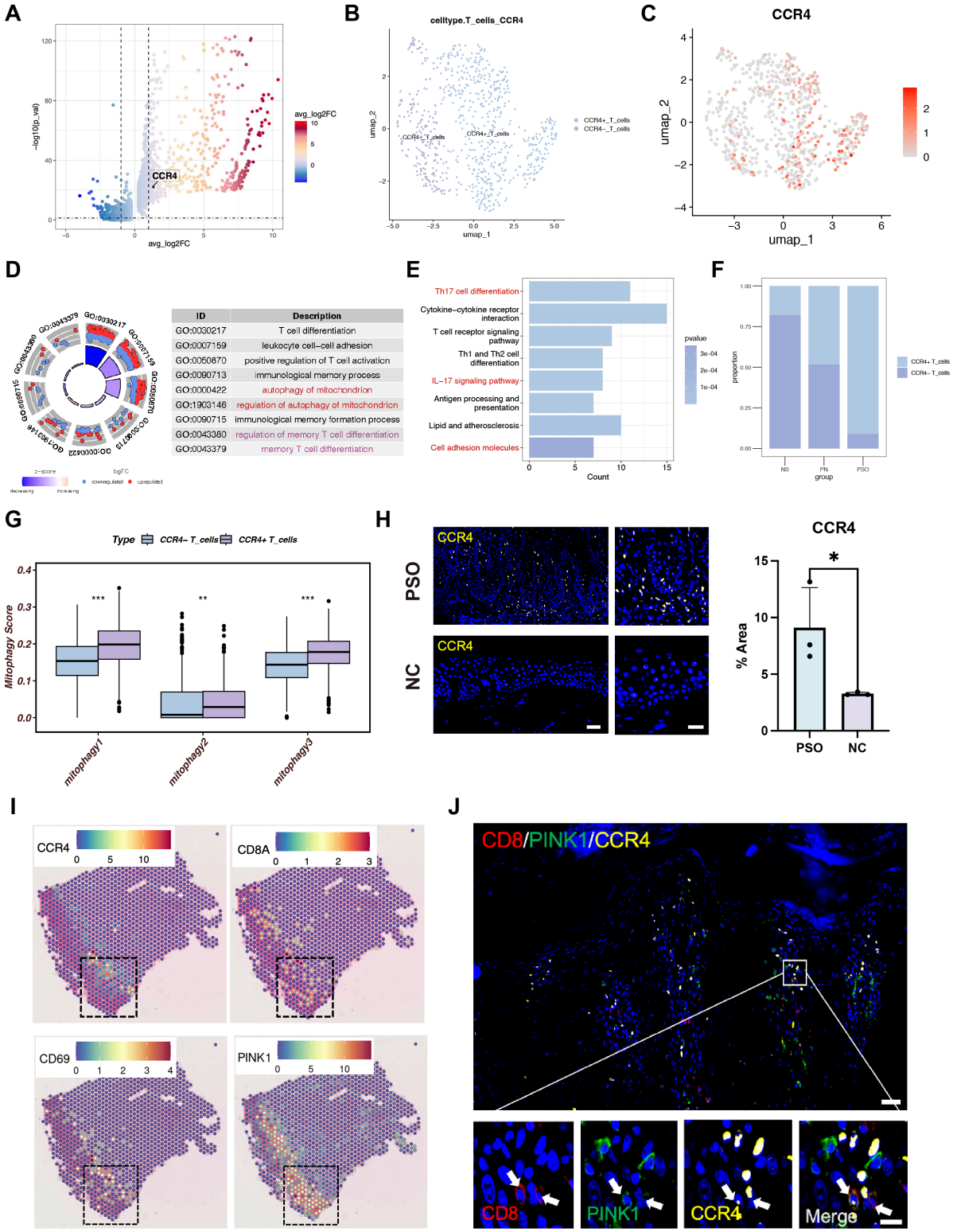

ID	Description
GO:0030217	T cell differentiation
GO:0007159	leukocyte cell–cell adhesion
GO:0050870	positive regulation of T cell activation
GO:0090713	immunological memory process
GO:0000422	autophagy of mitochondrion
GO:1903146	regulation of autophagy of mitochondrion
GO:0090715	immunological memory formation process
GO:0043380	regulation of memory T cell differentiation
GO:0043379	memory T cell differentiation

Figure 5

Single-cell and spatial analyses identify *CCR4* as a distinct marker for mitophagy^{hi} T cells co-localizing with PINK1^{+} CD8^{+} T cells in psoriasis. A) Volcano plot displaying differentially expressed genes (DEGs) in specific T cell subsets, with *CCR4* highlighted as a significantly upregulated gene. **B, C)** UMAP embeddings demonstrating the sub-clustering of T cells into CCR4^{+} and CCR4^{-} populations **(B)**, and the continuous expression profile of the *CCR4* transcript at single-cell resolution **(C)**. **D)** Gene Ontology (GO)

enrichment analysis of the DEGs, indicating significant enrichment in biological processes. **E)** KEGG pathway enrichment analysis highlighting key pathways associated with the $CCR4^+$ T cell subset. **F)** Bar graph showing the relative proportions of $CCR4^+$ and $CCR4^-$ T cells across different skin statuses (NS: normal skin, PN: non-lesional skin, PSO: Psoriasis). **G)** Box plots comparing various mitophagy scoring modules (mitophagy1, mitophagy2, mitophagy3) between $CCR4^-$ and $CCR4^+$ T cell subsets. *** $P < 0.001$, **** $P < 0.0001$. **H)** Representative immunofluorescence images and corresponding quantification of CCR4 protein expression in psoriasis (PSO) and normal control (NC) skin tissues. Scale bars: 50 μm, enlarged scale bar: 20 μm.* $P < 0.05$. **I)** Spatial transcriptomics feature plots illustrating the *in situ* expression and high spatial co-occurrence of *CCR4*, *CD8A*, *CD69*, and *PINK1* transcripts in human skin tissue. Dashed boxes highlight regions of strong spatial overlap. **J)** Representative multiplex immunofluorescence images evaluating the spatial co-localization of CD8 (red), PINK1 (green), and CCR4 (yellow). Scale bars: 500 μm, enlarged scale bar: 20 μm. All quantitative data are presented as mean ± SEM.

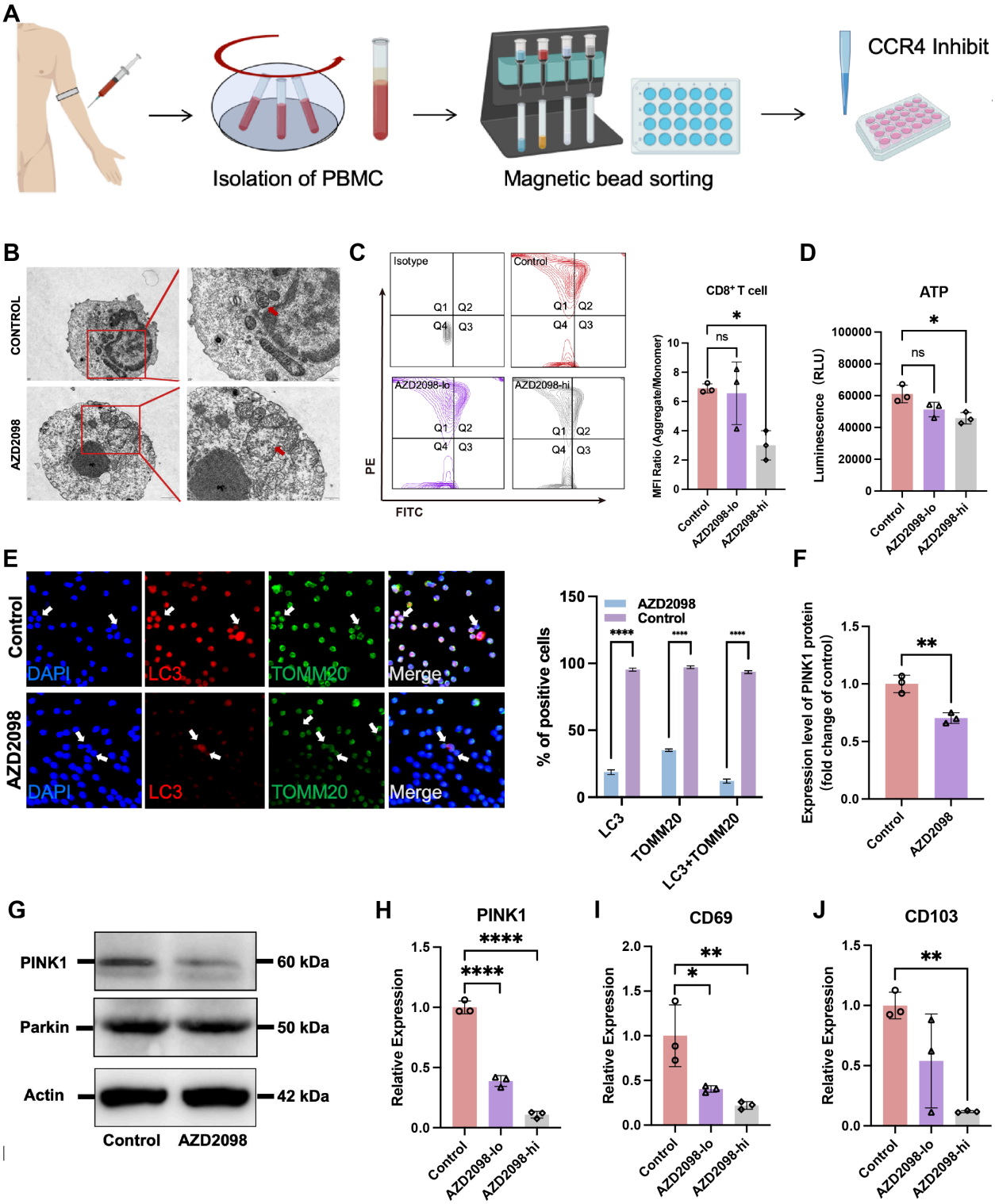

Figure 6

Pharmacological inhibition of CCR4 suppresses mitophagy and downregulates residency markers in human primary CD8⁺ T cells. A) Schematic illustration of the *in vitro* experimental design. Human PBMCs were isolated, and CD8⁺ T cells were enriched via magnetic bead sorting before treatment with the CCR4 inhibitor AZD2098. **B)** Representative transmission electron microscopy images showing the ultrastructure of Control and AZD2098-treated CD8⁺ T cells. **C)** Representative flow cytometry contour

plots (left) and quantitative analysis of the Mean Fluorescence Intensity (MFI) ratio (right) evaluating mitochondrial membrane potential in $CD8^+$ T cells treated with low-dose AZD2098 (AZD2098-lo), or high-dose AZD2098 (AZD2098-hi). **D)** ATP levels in $CD8^+$ T cells across the indicated treatment groups. **E)** Representative immunofluorescence images (left) and quantitative analysis (right) evaluating the co-localization of the autophagosome marker LC3 (red) and the mitochondrial marker TOMM20 (green) in Control and AZD2098-treated cells. White arrows indicate areas of LC3 and TOMM20 co-localization, indicative of active mitophagy. **F,G)** Western blot analysis **(G)** and quantification **(F)** of PINK1 protein expression in $CD8^+$ T cells treated with or without AZD2098. Parkin expression is also shown in **(G)**. Actin served as an internal loading control. **H–J)** Relative mRNA expression levels of *PINK1* **(H)**, *CD69* **(I)**, and *CD103* **(J)** in primary $CD8^+$ T cells treated with AZD2098-lo or AZD2098-hi. Data are presented as mean ± SEM of independent biological replicates. ns, not significant; * $P < 0.05$, ** $P < 0.01$, *** $P < 0.001$, **** $P < 0.0001$.

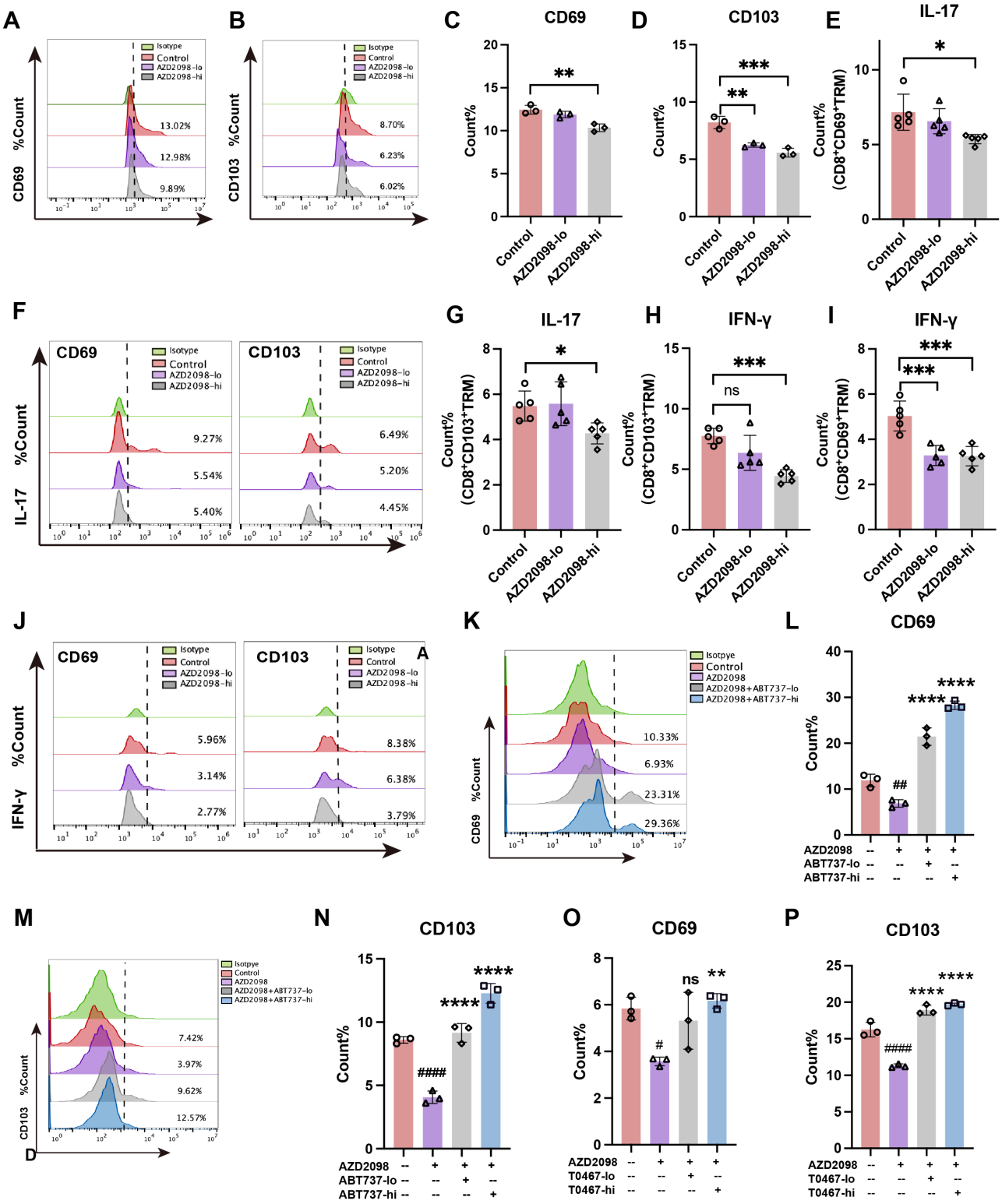

Figure 7

The CCR4-PINK1 axis critically regulates the phenotypic maintenance and effector functions of human CD8+ TRM. A, B) Representative flow cytometry histograms depicting the surface expression of CD69 **(A)** and CD103 **(B)** on primary $CD8^+$ T cells treated with vehicle (Control), low-dose AZD2098 (AZD2098-lo), or high-dose AZD2098 (AZD2098-hi). **C, D)** Quantitative analysis of the percentage of $CD8^+CD69^+$ **(C)** and $CD8^+CD103^+$ **(D)** cells from panels (A) and (B). **F, J)** Representative flow cytometry histograms

analyzing the intracellular expression of the effector cytokines IL-17 **(F)** and IFN- gamma **(J)** within the $CD8^+CD69^+$ (left) and $CD8^+CD103^+$ (right) TRM subpopulations across the indicated treatment groups. **E, G)** Statistical quantification of the percentage of IL-17-producing cells within the $CD8^+CD69^+$ **(E)** and $CD8^+CD103^+$ **(G)** TRM subsets. **H,I)** Statistical quantification of the percentage of IFN-γ-producing cells within the $CD8^+CD103^+$ **(H)** and $CD8^+CD69^+$ **(I)** TRM subsets. **K–N)** Phenotypic rescue using the PINK1 activator ABT737. Representative flow cytometry histograms **(K, M)** and quantitative analysis of the percentage of $CD69^+$ **(L)** and $CD103^+$ **(N)** cells. $CD8^+$ T cells were treated with AZD2098 alone or in combination with low/high doses of ABT737. **O-P)** Phenotypic rescue using the PINK1 activator T0467. Quantitative analysis of the percentage of $CD69^+$ **(O)** and $CD103^+$ **(P)** cells in $CD8^+$ T cells treated with AZD2098 alone or in combination with low/high doses of T0467. Data are presented as mean ± SEM of independent biological replicates. ns, not significant; * $P < 0.05$, ** $P < 0.01$, *** $P < 0.001$, **** $P < 0.0001$ compared to the AZD2098-only group. # $P < 0.05$, ## $P < 0.01$, #### $P < 0.0001$ compared to the Control group.

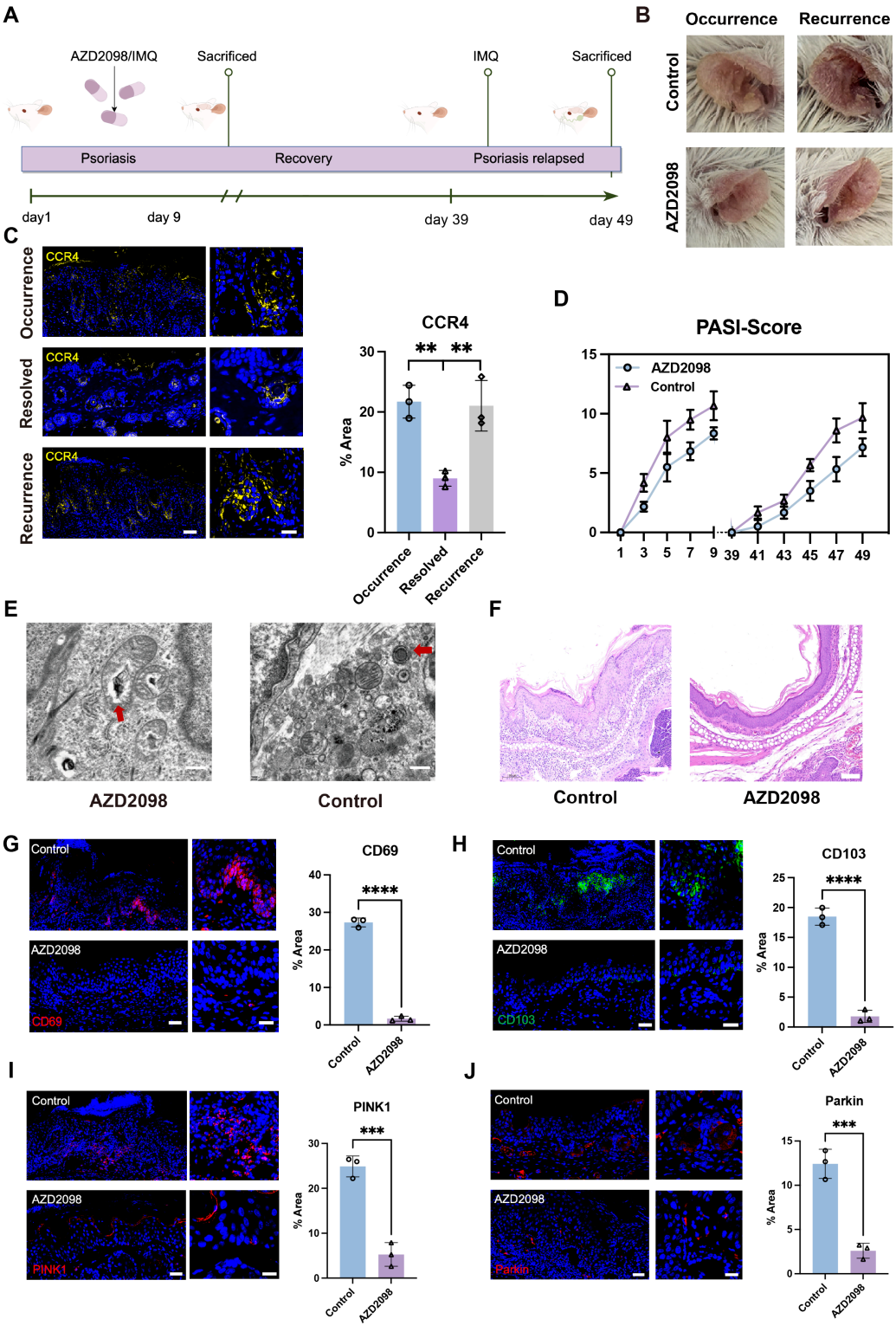

Figure 8

Pharmacological blockade of CCR4 attenuates psoriasis-like lesions and suppresses mitophagy-mediated T cell residency. A) Schematic representation of the *in vivo* experimental timeline. Mice were treated with topical IMQ alongside systemic administration of the CCR4 inhibitor AZD2098 during the initial induction (occurrence phase), followed by a recovery period and a subsequent IMQ rechallenge (recurrence phase). **B)** Representative macroscopic phenotypic images of the ear skin from Control and

AZD2098-treated mice during the occurrence and recurrence phases. **C)** Representative immunofluorescenceimages (left) and quantitative analysis (right) showing the dynamic expression of CCR4 (yellow) in skin tissues during the occurrence, resolved, and recurrence phases of the disease model. ** $P < 0.01$. **D)**Clinical evaluation of disease severity by tracking PASI scores over the 49-day experimental timeline for both the Control and AZD2098-treated groups. **E)**Representative transmission electron microscopy images revealing the ultrastructural changes in the skin tissues of AZD2098-treated and Control mice. **F)** Representative H&E staining of ear skin sections, demonstrating reduced epidermal hyperplasia and inflammatory infiltration in the AZD2098 treatment group compared to the Control. **G–J)** Representative immunofluorescence images (left) and quantitative analysis of the fluorescence-positive area percentages (right) for CD69 (**G**) and CD103 (**H**), as well as the mitophagy-related proteins PINK1 (**I**) and Parkin (**J**) in lesions of Control and AZD2098-treated mice. Scale bars: 50 μm, enlarged scale bar: 20 μm. All quantitative data are presented as mean ± SEM. *** $P < 0.001$, **** $P < 0.0001$.

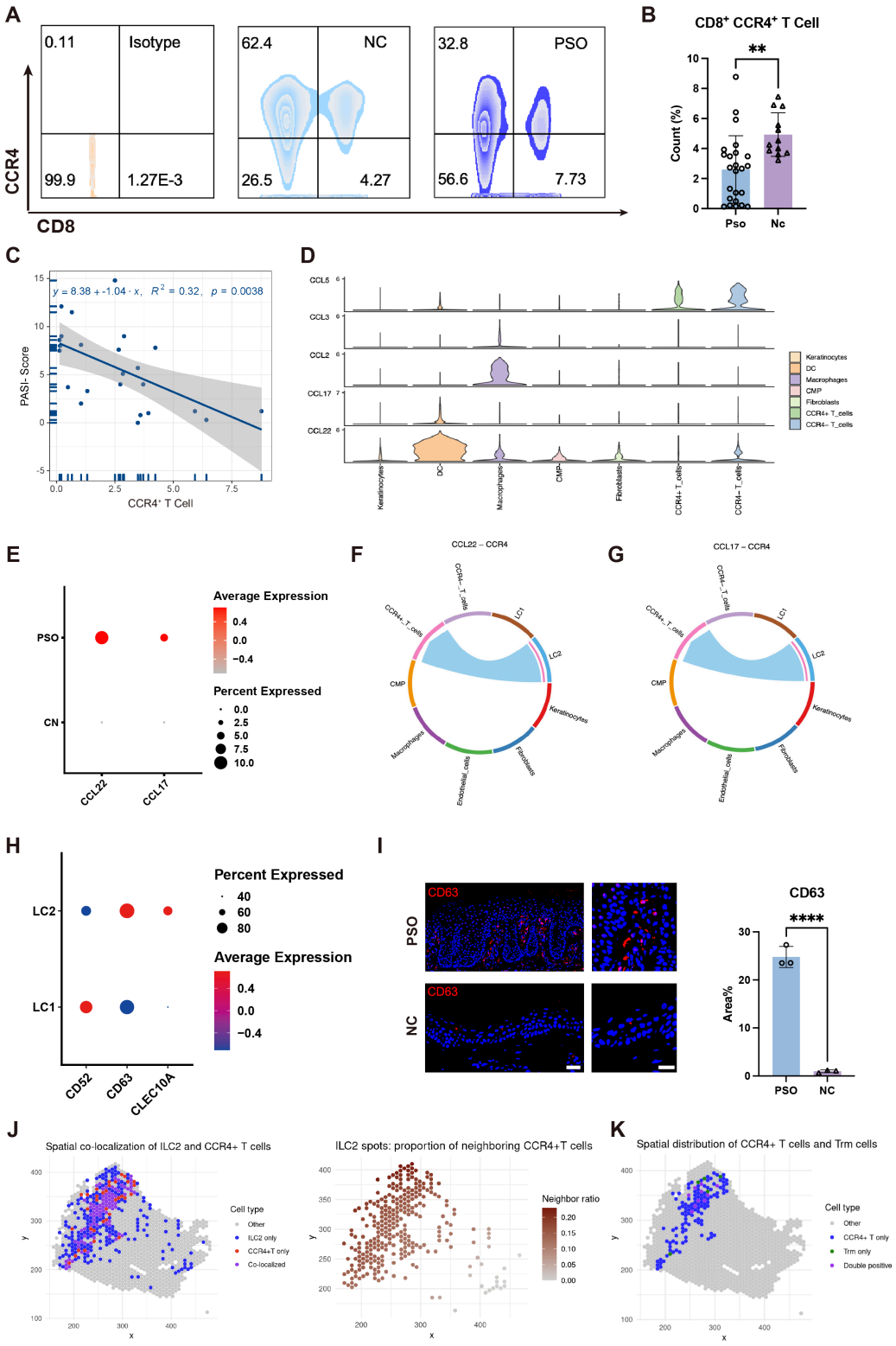

Figure 9

The CCL17/22-CCR4 axis mediates the recruitment of CCR4$^+$ T cells by Langerhans cells in psoriasis. **A, B)** Representative flow cytometry contour plots **(A)** and statistical quantification **(B)** comparing the percentage of CD8$^+$CCR4$^+$ T cells (isolated from human PBMCs) between patients with psoriasis (PSO) and normal controls (NC). $^{**}P < 0.01$. **C)** Pearson correlation analysis revealing a significant negative correlation between the proportion of CD8$^+$CCR4$^+$ T cells (isolated from human PBMCs) and PASI scores

(R^2 = 0.32, *p* = 0.0058). The shaded area represents the 95% confidence interval. **D)** Violin plots derived from scRNA-seq data showing the expression distribution of various chemokines. **E)** Dot plot illustrating the average expression levels and expressing cell proportions of *CCL17* and *CCL22* in psoriatic lesions versus controls (CN). **F, G)** Circos plots inferring intercellular communication networks based on ligand-receptor interactions. The plots specifically highlight the signaling from DCs to $CCR4^+$ T cells via the CCL17-CCR4 **(F)** and CCL22-CCR4 **(G)** pathways. **H)** scRNA-seq dot plot identifying specific marker genes (*CD52*, *CD63*, *CLEC10A*) used to distinguish Langerhans cell (LC) subclusters LC1 and LC2. **I)** Representative immunofluorescence images (left) and quantification (right) of CD63 protein expression (red) in PSO and NC skin tissues. Scale bars: 50 μm, enlarged scale bar: 20 μm. **** $P < 0.0001$. **J)** Spatial transcriptomics feature plots mapping the spatial co-localization of the LC2 subset and $CCR4^+$ T cells (left), alongside the nearest-neighbor proportion analysis of LC2 spots adjacent to CCR4+ T cells (right). **K)** Spatial transcriptomics feature plot demonstrating the *in situ* spatial co-distribution and overlap (double-positive spots) between CCR4+ T cells and TRM cells in the psoriatic microenvironment. All quantitative data are presented as mean ± SEM.

Supplementary Files

This is a list of supplementary files associated with this preprint. Click to download.

- XXactin.tif24bit.tif
- PINK1.tif24bit.tif
- Supportinginformation.docx
- Parkin.tif24bit.tif